Journal of Solid State Chemistry **154,** 498–506 (2000)
doi:10.1006/jssc.2000.8870, available online at http://www.idealibrary.com on IDEAL®

Vibrational and X-Ray Studies of the Polymorphic Forms of $LiIn(MoO_4)_2$

M. Mączka,[1] J. Hanuza, and A. Pietraszko

Institute for Low Temperature and Structure Research, Polish Academy of Sciences, P.O. Box 1410, 50-950 Wrocław 2, Poland

Received April 18, 2000; in revised form June 14, 2000; accepted July 13, 2000; published online September 30, 2000

IR and Raman studies of the low- and high-temperature phases of $LiIn(MoO_4)_2$ were performed at ambient temperature. The crystal structure of the low-temperature modification was solved. The observed vibrational modes were assigned to the vibrations of respective atoms in the unit cells. The origin of brown coloration and unusual shift of stretching vibrations toward higher energy, observed for the low-temperature polymorph, were explained as a result of instability of wolframite-type structure containing MoO_6 octahedra. © 2000 Academic Press

Key Words: **double molybdates; vibrational spectra; phase transition.**

INTRODUCTION

Metal molybdates and tungstates represent a large class of inorganic compounds, which have found application in the field of heterogeneous catalysis and quantum electronics (1–3). Many of these compounds exhibit also ferroelectric and ferroelastic properties (4–6). The discussed compounds may crystallize in a very wide number of structures, which may be regarded as originating from either the structure of scheelite ($CaWO_4$), with isolated MoO_4^{2-} (WO_4^{2-}) tetrahedra, or the structure of wolframite, with octahedral coordination of hexavalent atoms. For simple molybdates and tungstates, of the formula $M^{II}M^{VI}O_4$, the scheelite-type structures are stable if the difference in the ionic radius of Mo^{VI} (W^{VI}) and the bivalent cation M^{II} is large, whereas the octahedral coordination is realized when this difference is small (7). Therefore, the wolframite-type tungstates are formed only for bivalent cations with ionic radii smaller than 0.97 Å, i.e., for Fe, Mn, Co, Ni, Mg, Zn, Cd (7). In case of double tungstates, with the general formula $M^{I}M^{III}(WO_4)_2$, the wolframite-type structures were reported for M^{I} = Li, Na and M^{III} = In, Sc, Fe (8,9). Because of smaller ionic radius of Mo^{VI}, when compared with W^{VI} (10), simple molybdates may crystallize in structures built of MoO_6 octahedra if the ionic radius of the bivalent cation is smaller than 0.77 Å, i.e., for Fe, Ni, Co (7). However, the formed crystal structure is not similar to that of wolframite (1, 11, 12). Moreover, even for these small bivalent cations the crystal structure may be transformed at high temperatures into the structure with tetrahedral coordination of Mo atoms (1, 13).

In the present paper we are going to report on vibrational studies of the low- and high-temperature phases of $LiIn(MoO_4)_2$. This double molybdate is an interesting material for investigation since it is the only known representative of a very large family of double molybdates, which was reported to crystallize at ambient temperature with octahedral coordination of Mo atoms and which exhibits a high-temperature phase transition into a structure with isolated MoO_4^{2-} tetrahedra. We will show that the low-temperature structure of $LiIn(MoO_4)_2$ is different from that of simple molybdates with Fe, Ni, and Co atoms; i.e., $LiIn(MoO_4)_2$ crystallizes in the typical wolframite-type structure and is isostructural to $LiIn(WO_4)_2$.

EXPERIMENTAL

Single crystals of the low-temperature polymorph were grown by the flux method developed by Klevtsov *et al.* (14). The cooling rate was 2°C/h and the obtained crystals were pale brown. The high-temperature phase was obtained by heating a small amount of the obtained crystals to 750°C in a platinum crucible and then by cooling to ambient temperature at a rate of 10°C/min. The obtained colorless crystals were very small, with dimensions less than 0.5 mm. The purity of the both phases was checked by measuring the powder X-ray diffraction pattern using a Stoe powder diffraction system, employing Cu$K\alpha$ radiation. The measured diffraction pattern for the low-temperature structure was identical to that reported in Ref. 15. Since there are no literature data concerning the X-ray powder diffraction data for the high-temperature phase, the measured diffractogram was compared with that calculated from the single-crystal data, reported in Ref. 16. The recorded and calculated

[1] To whom correspondence should be addressed. Fax: 48 + 71-441029. E-mail: maczka@int.pan.wroc.pl.

0022-4596/00 $35.00

patterns were identical, indicating that the obtained sample is very pure.

A single crystal of the low-temperature phase of $LiIn(MoO_4)_2$ was investigated by the X-ray diffraction method. Data for the structure determination were collected on a KM-4 KUMA single-crystal diffractometer with graphite-monochromated Mo$K\alpha$ radiadion ($\lambda = 0.71073$ Å). Lattice parameters were determined by least-squares refinement of the setting angles for 30 selected reflections.

IR spectra were recorded with a Biorad FT-IR spectrometer. The polycrystalline spectra were measured in KBr suspension in the region 1100–450 cm^{-1} and in nujol suspension in the region 600–30 cm^{-1}. Raman spectra were recorded in the region 1100–100 cm^{-1} with a Brukker FT-Raman spectrometer and the 1064-nm excitation. In the low-frequency region, below 200 cm^{-1}, the Raman spectra were obtained with a TH1000 Ivon Jobin spectrometer and 514.5 nm excitation. All spectra were recorded with a resolution of 2 cm^{-1}.

RESULTS AND DISCUSSION

Low-Temperature Phase Structure Determination

A total of 5559 reflections in a range $2^\circ < 2\theta < 101^\circ$ were collected using a ω-θ scan technique, with prescanning and a scan speed depending on the intensity (0.02 to 0.1°/min), and scan range (ω) 1.3°. No significant intensity variation was observed for two standard reflections monitored every 50 measured reflections. After merging ($R_{int} = 0.0525$) 2849 independent reflections, 2226 with $F > 4\sigma(F)$ were used for the structure determination. Lorenz, polarization, and absorption correction were applied. Empirical absorption correction was based on ψ scans of selected reflections. The extinction was introduced in the refinement. The SHELX97 (PC version) program was used for all the structure calculations (17).

The $LiIn(MoO_4)_2$ crystals have a monoclinic symmetry (space group $C2/c$) with four chemical units ($Z = 4$) forming the room temperature cell. Lattice parameters at room temperature are the following: $a = 9.504(1)$, $b = 11.459(1)$,

TABLE 1
Crystal Data and Structure Refinement for the Low-Temperature Phase of $LiIn(MoO_4)_2$

Empirical formula	In Li Mo_2 O_8
Formula weight	441.64
Temperature	293(2) K
Wavelength	0.71073 Å
Crystal system, space group	monoclinic, $C2/c$
Unit cell dimensions	$a = 9.504(2)$ Å, $\alpha = 90^\circ$
	$b = 11.459(2)$ Å, $\beta = 91.49(3)^\circ$
	$c = 4.9940(10)$ Å, $\gamma = 90^\circ$
Volume	543.69(18) $Å^3$
Z, calculated density	4, 5.395 Mg/m^3
Absorption coefficient	8.749 mm^{-1}
$F(000)$	800
Crystal size	$0.2 \times 0.23 \times 0.16$ mm
θ Range for data collection	2.78 to 50.16
Limiting indices	$-20 \le h \le 20, 0 \le k \le 24,$
	$-10 \le l \le 10$
Reflections collected/unique	5559/2849 [R(int) = 0.0525]
Completeness to $\theta = 50.16$	48.1%
Refinement method	Full-matrix least-squares on F^2
Data/restraints/parameters	2849/0/57
Goodness-of-fit on F^2	1.284
Final R indices [$I > 2\sigma(I)$]	$R1 = 0.0412$, $\omega R2 = 0.1067$
R indices (all data)	$R1 = 0.0457$, $\omega R2 = 0.1093$
Extinction coefficient	0.0102(7)
Largest diff. peak and hole	7.992 and -4.870 e. $Å^{-3}$

TABLE 2
Atomic Coordinates ($\times 10^4$) and Equivalent Isotropic Displacement Parameters ($Å^2 \times 10^3$) for $LiIn(MoO_4)_2$

	x	y	z	U(eq)
In(1)	0	9072(1)	2500	4(1)
Mo(1)	2681(1)	8425(1)	−2496(1)	3(1)
Li(1)	5000	9071(18)	2500	38(5)
O(1)	1227(2)	9358(2)	−3893(4)	5(1)
O(2)	3529(2)	7000(2)	−666(4)	6(1)
O(3)	3620(2)	8065(2)	−5425(4)	6(1)
O(4)	3756(2)	9414(2)	−925(4)	8(1)

Note. U(eq) is defined as one-third of the trace of the orthogonalized U_{ij} tensor.

TABLE 3
Selected Bond Lengths (Å) for $LiIn(MoO_4)_2$

In(1)–O(2)[a]	2.0903(17)
In(1)–O(2)[b]	2.0903(17)
In(1)–O(2)[c]	2.1455(19)
In(1)–O(2)[d]	2.1455(19)
In(1)–O(2)[e]	2.2635(18)
In(1)–O(2)[f]	2.2635(18)
In(1)–In(1)[g]	3.2794(5)
Mo(1)–O(4)	1.7031(19)
Mo(1)–O(3)	1.7817(19)
Mo(1)–O(1)	1.8675(17)
Mo(1)–O(2)	2.0284(18)
Mo(1)–O(2)[a]	2.0362(18)
Mo(1)–O(3)[h]	2.3361(19)
Mo(1)–Li(1)	3.368(5)
Li(1)–O(3)[i]	2.048(12)
Li(1)–O(3)[d]	2.048(12)
Li(1)–O(4)[j]	2.091(4)
Li(1)–O(4)	2.091(4)
Li(1)–O(4)[k]	2.254(16)
Li(1)–O(4)[e]	2.254(16)
Li(1)–Li(1)[i]	3.28(3)

Note. Symmetry transformations used to generate equivalent atoms: [a] $-x+1/2, -y+3/2, z$. [b] $x-1/2, -y+3/2, z+1/2$. [c] $-x, y, -z-1/2$. [d] $x, y, z+1$. [e] $x, -y+2, z+1/2$. [f] $-x, -y+2, -z$. [g] $-x, -y+2, -z+1$. [h] $-x+1/2, -y+3/2, -z-1$. [i] $-x+1, y, -z-1/2$. [j] $-x+1, y, -z+1/2$. [k] $-x+1, -y+2, -z$. [i] $-x+1, -y+2, -z+1$.

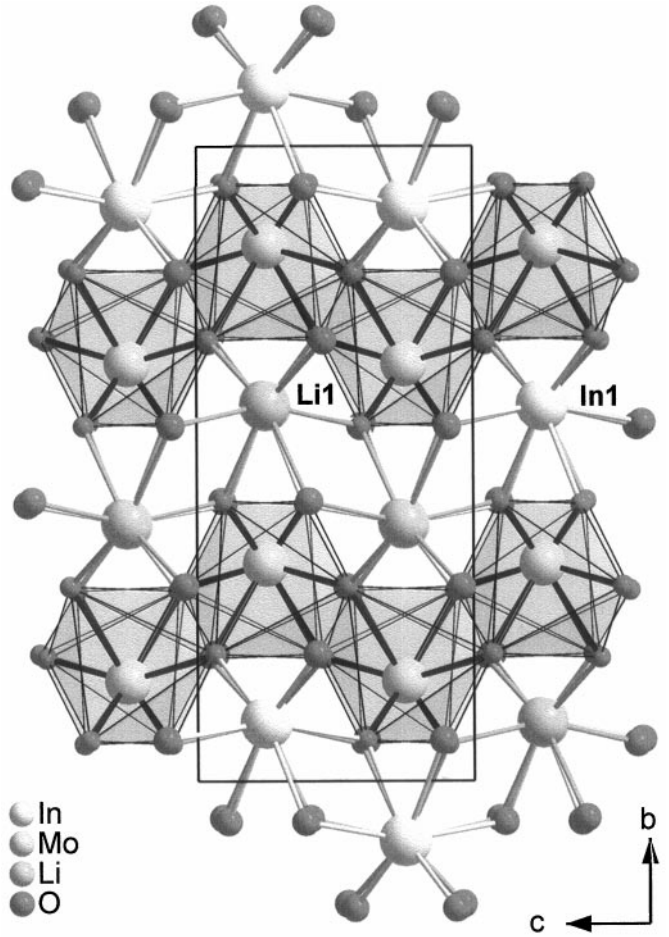

FIG. 1. The crystal structure of the low-temperature phase of $LiIn(MoO_4)_2$ projected on *yz* plane.

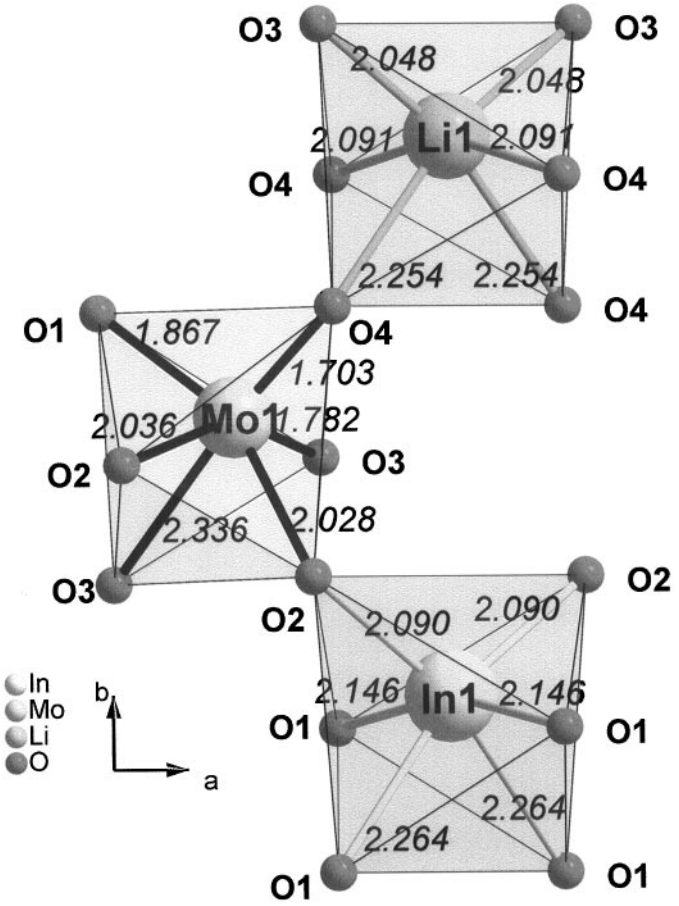

FIG. 2. The projection of the arrangement of the polyhedra for In, Li and Mo on *xy* plane.

$c = 4.994(1)$ Å, $\beta = 91.49^\circ$, $V = 543.69(2)$ Å^3 (see Table 1). The final discrepancy factor is $R = 0.0412$. Final coordinates and equivalent isotropic displacement coefficients with e.s.d.s in parentheses are presented in Table 2, and selected interatomic distances in Table 3. The crystal structure of $LiIn(MoO_4)_2$ projected on *yz* plane is shown in Fig. 1 and the projection of the arrangement of the polyhedra for In, Li, and Mo projected on *xy* plane is shown in Fig. 2.

High-Temperature Phase of $LiIn(MoO_4)_2$

The high-temperature modification of $LiIn(MoO_4)_2$ is stable above 700°C (16) but it may be easily quenched to ambient temperature. Its crystal structure is monoclinic, $P2_1/c$, and the unit cell contains four molecular units (16). All atoms are situated in general positions and the MoO_4^{2-} ions occupy two sets of nonequivalent sites. The results of factor group analysis are shown in Table 4 and the recorded

TABLE 4
Factor Group Analysis for the High-Temperature Phase of $LiIn(MoO_4)_2$ ($P2_1/c$, $Z = 4$)

C_{2h}	E	C_2(b)	i	σ_h	n(N)	$n(T'(\mathrm{Li}))$	$n(T'(In))$	$n(T'(MoO_4))$	$n(L)$	n(int)	Activity IR	Activity Raman
A_g	1	1	1	1	36	3	3	6	6	18	—	xx, yy, zz, xz
B_g	1	−1	1	−1	36	3	3	6	6	18	—	xy, yz
A_u	1	1	−1	−1	36	3	3	6	6	18	y	—
B_u	1	−1	−1	1	36	3	3	6	6	18	x, z	—

Note. n(N) denotes the total number of modes; $n(T'(\mathrm{Li}))$, $n(T'(\mathrm{In}))$, and $n(T'(MoO_4))$ denote the number of translational modes of Li^+, In^{3+}, and MoO_4^{2-} ions, respectively; n(L) and n(int) denote the number of librational and internal modes, respectively.

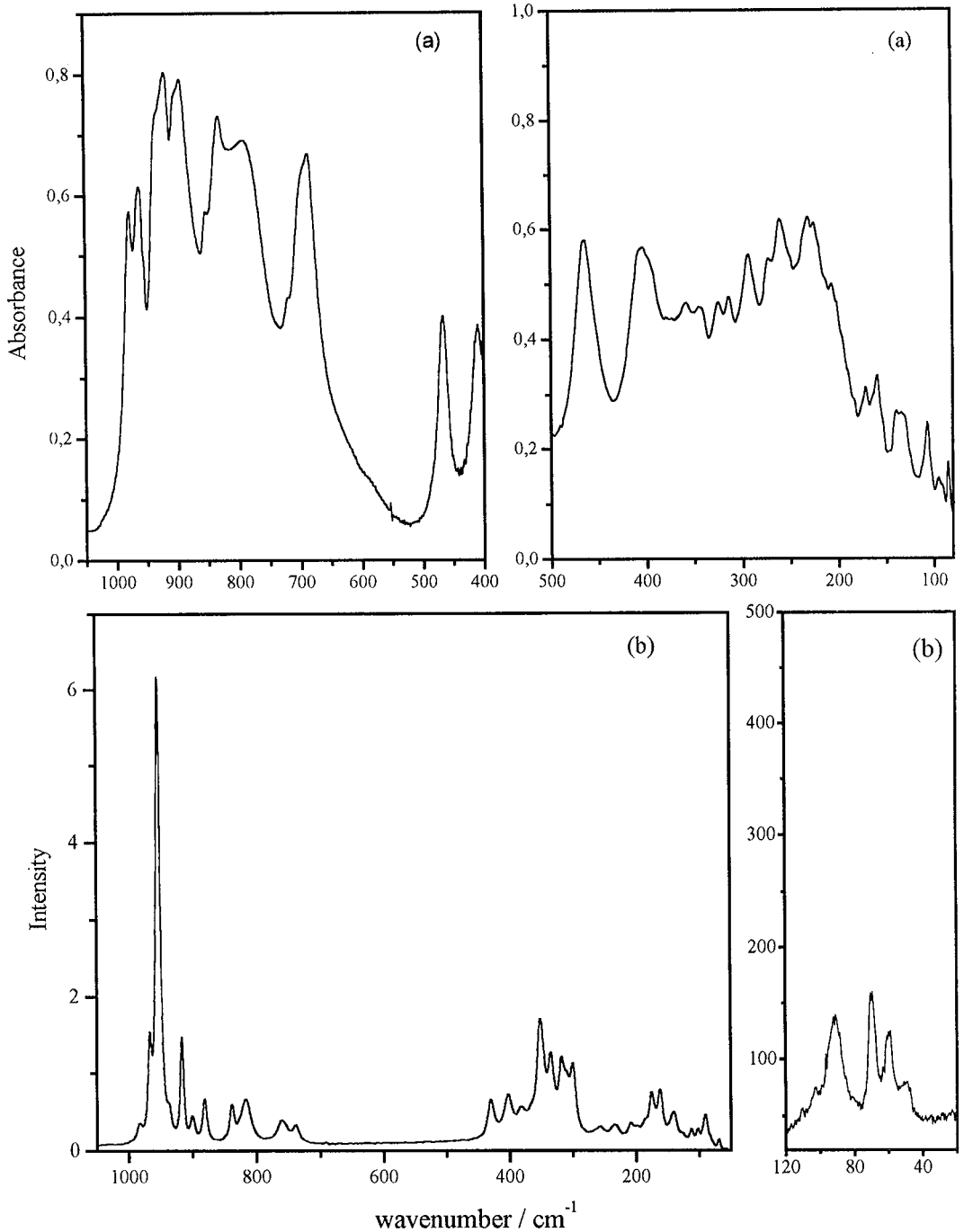

FIG. 3. (a) IR and (b) Raman spectra of the high-temperature phase of $LiIn(MoO_4)_2$.

IR and Raman spectra are presented in Fig. 3. The vibrational frequencies and the proposed assignment are shown in Table 5. The number of well-resolved peaks in the Raman spectrum, 34, and IR spectrum, 33, is approximately half of that predicted, indicating that for the majority of modes the Davydov splitting is very small and cannot be observed for the polycrystalline samples. The stretching modes region is well-separated from the lattice and bending modes, in agreement with the X-ray analysis showing that the coordination of the Mo atoms is tetrahedral. However, the observed frequency range of stretching modes is unusually broad and this may be attributed to the large distortion of the MoO_4^{2-} tetrahedra. The X-ray analysis shows that although one of the MoO_4^{2-} tetrahedra is rather weakly distorted, the second independent MoO_4^{2-} ion shows a large distribution of Mo–O bond lengths, which change from 1.701(3) to 1.862(3)

TABLE 5
Measured Vibrational Modes (in cm^{-1}) for the High-Temperature Phase of $LiIn(MoO_4)_2$ Together with Literature Data for $LiAl(MoO_4)_2$ (19)

$LiIn(MoO_4)_2$		$LiAl(MoO_4)_2$		
IR	Raman	IR	Raman	Assignment
—	983vw	—	—	Overtone
978m	966m	972sh	977m	$\nu_s(MoO_4)$
961m	952vs	963s	957vs	$\nu_s(MoO_4)$
—	938vw	—	—	overtone
930sh	916m	948m	929m	$\nu_{as}(MoO_4)$
919s	900w	902w	900m	$\nu_{as}(MoO_4)$
899sh	—	—	—	$\nu_{as}(MoO_4)$
895s	881w	857s	861w	$\nu_{as}(MoO_4)$
853w	—	—	—	overtone
832s	839w	807s	835w	$\nu_{as}(MoO_4)$
792s	817m	750m	806w	$\nu_{as}(MoO_4)$
693sh	761w	—	—	overtone?
686s	738w	700s	744w	$\nu_{as}(MoO_4)$
466m	431w	510s	518w	
404m	403w	426m	487w	$\delta_{as}(MoO_4)$,
400sh	383w	399m	451w	$T'(Li^+)$, and $T'(Al^{3+})$
—	—	369m	424w	
359w	352m	359w	403m	
343w	335m	331w	380s	$\delta_s(MoO_4)_2$ and
325w	318m	—	331w	$T'(Li^+)$
314w	313w	305m	317w	
293m	301m	282sh	295m	
273w	—	—	266m	
260m	257w	251m	238w	$T'(In^{3+})$ and
231m	234w	—	—	$T'(MoO_4)$
225m	209w	204m	200m	
207w	199vw	—	196sh	
—	183vw	—	—	
172w	176m	176w	—	
164sh	162m	—	174m	
159w	140m	—	155m	
153sh	127vw	137w	142w	$L(MoO_4)$ and
140w	113w	127w	128vw	$T'(MoO_4)$
135w	102w		115m	
107w	91m		89m	
94w	70m			
85w	60m	75w	82m	
	50w			

Å (16). Such a large difference in bond lengths may be the result of interactions between the adjacent ions, which lead to formation of weak Mo–O ⋯ Mo bridging bonds. Such weak bonds, with the Mo ⋯ O distance of 2.43(3) Å, were found in $LiAl(MoO_4)_2$ crystal, which has a crystal structure very similar to that of $LiIn(MoO_4)_2$ (16,18). Because of the similarity of the crystal structures of the both molybdates, it is reasonable to compare their vibrational properties in order to facilitate the assignment of the observed modes. This is especially useful in our case since the vibrational spectra of $LiAl(MoO_4)_2$ were studied in detail and the vibrational assignment was proposed on the basis of phonon calculation and isotopic substitution (19).

Such a comparison permits straightforward assignment of the majority of stretching modes (see Table 5). It should be noticed, however, that the spectra of $LiIn(MoO_4)_2$ show the presence of more vibrational modes than the spectra recorded for $LiAl(MoO_4)_2$. These additional weak bands, observed at 983, 938, and 853 cm^{-1}, may be assigned most likely to overtones or combination modes. The origin of the 761 cm^{-1} Raman band is not clear since its intensity seems to be too high for an overtone. Moreover, the frequency difference between this mode and the 738 cm^{-1} line seems to be too large to permit the assignment of these two modes as a Davydov doublet.

The comparison of the low-frequency spectra of $LiAl(MoO_4)_2$ and $LiIn(MoO_4)_2$ allows us to conclude that the bending vibrations give rise to the bands observed in the 290–470 cm^{-1} region. The translational modes of Li^+ and MoO_4^{2-} ions, i.e., $T'(Li^+)$ and $T'(MoO_4^{2-})$, and librational modes ($L(MoO_4)$) are observed in the 290–470, 50–280, and 50–180 cm^{-1} regions, respectively. The remaining modes, describing translational motions of In^{3+} ions, may be located on the basis of vibrational studies of $LiAl(MoO_4)_2$ (19) and a few other alkali ion–indium and –aluminium tungstates and molybdates (20, 21). These studies show that the substitution of Al^{3+} ions by much heavier In^{3+} ions leads to frequency decrease from 400–500 to 200–250 cm^{-1}, respectively. We may assign, therefore, the multiplet in the 180–280 cm^{-1} range to the translational modes of In^{3+} ions coupled with $T'(MoO_4)$ phonons. The proposed assignment is further supported by the observation that in the 370–520 cm^{-1} range more modes are observed for $LiAl(MoO_4)_2$ than for $LiIn(MoO_4)_2$, whereas the opposite behavior is noticed in the 180–280 cm^{-1} range.

Phase Transition and the Vibrational Properties of the Low-Temperature Phase of $LiIn(MoO_4)_2$

$LiIn(MoO_4)_2$ exhibits a first-order phase transition at 700°C (16) and its low-temperature structure was reported to be similar to that of $LiIn(WO_4)_2$ and $LiFe(WO_4)_2$ (15, 22, 23), i.e., wolframite-type with MoO_4^{2-} ions connected each other to through double Mo⋯O⋯Mo oxygen bridges. The conclusion that $LiIn(MoO_4)_2$ is isostructural to the respective tungstates was derived from the similarity of their powder diffraction patterns. The results of the single-crystal X-ray study, presented in the previous section of this paper, confirm this conclusion. These results show that the first-order transition is without a group–subgroup relation and that as a result of the transition the structure of $LiIn(MoO_4)_2$ collapses, leading to 23.0% decrease in the unit cell volume.

The IR and Raman spectra of the low-temperature phase of $LiIn(MoO_4)_2$ (presented in Fig. 4) are also consistent with the conclusion that $LiIn(MoO_4)_2$ is isomorphous to $LiIn(WO_4)_2$ but has a different structure than simple molybdates. This is evidenced through the fact that the pattern and number of bands observed for $LiIn(MoO_4)_2$ are similar as found for the tungsten derivative (24, 25) (see Table 6), but are different than found for α-$CoMoO_4$ (see Ref. 11). Both spectra differ, however, significantly as far as the frequency and intensity of some modes is concerned. Before we discuss the origin of these differences, we will first assign the vibrational bands to the normal modes.

In wolframite-type structures all MoO_4^{2-} ions are connected to each other through the double oxygen bridges forming infinite chains along the *c*-axis. Therefore, as a basis for the factor group analysis a unit cell containing two Li^+,

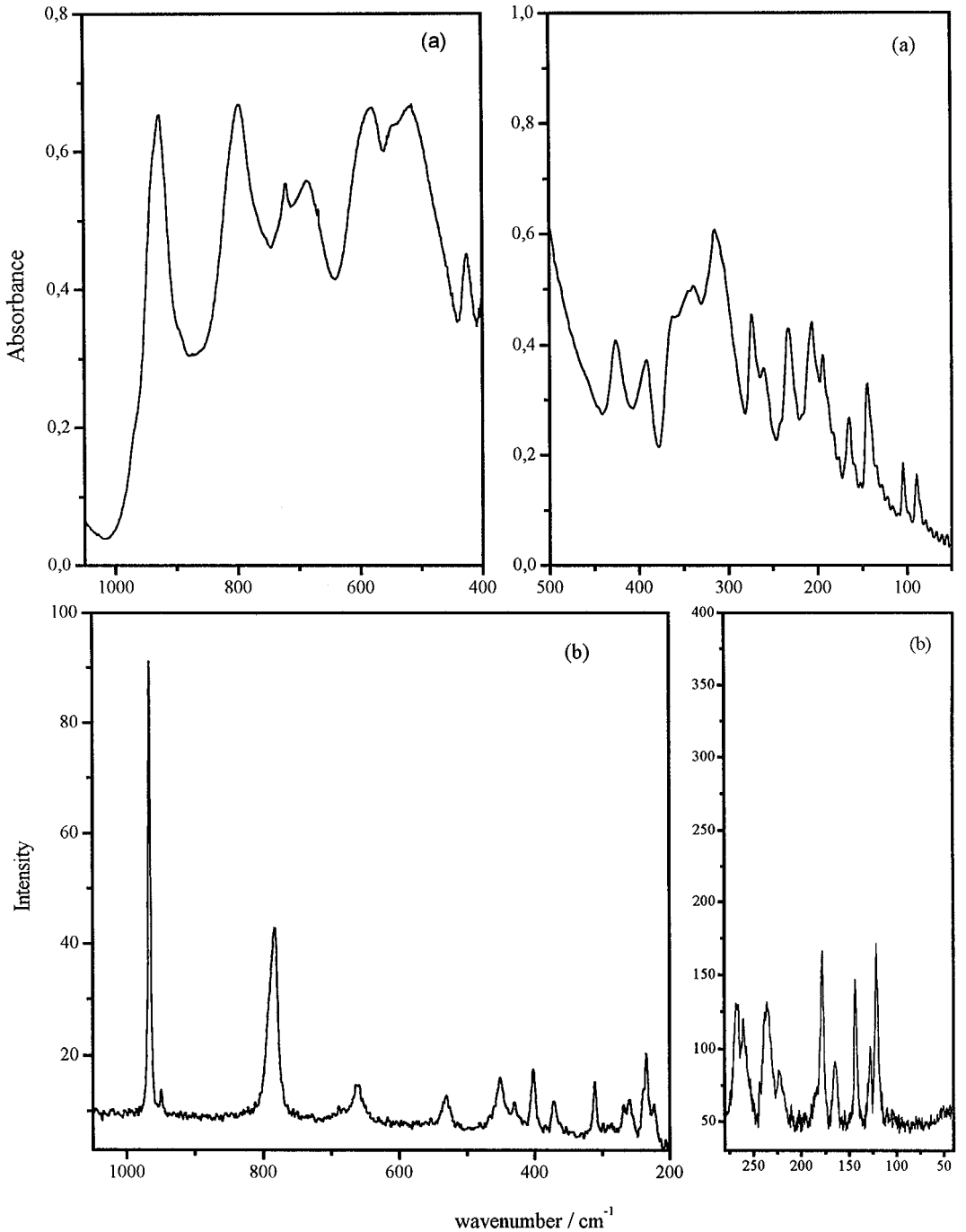

FIG. 4. (a) IR and (b) Raman spectra of the low-temperature phase of $LiIn(MoO_4)_2$.

TABLE 6
Measured Vibrational Modes (in cm^{-1}) for the Low-Temperature Phase of $LiIn(MoO_4)_2$ Together with Literature Data for $LiIn(WO_4)_2$ (25)

$LiIn(MoO_4)_2$		$LiIn(WO_4)_2$		
IR	Raman	IR	Raman	Assignment
940sh	—	940w	—	Mo–O terminal stretching modes
927s	966vs	908m	916vs	
—	949vw	—	—	
—	790sh	825s	793m	
797s	784s	—	775w	
685m	689w	738sh	—	Bridging stretching modes
—	—	716s	716w	
580s	661w	648m	675w	
—	—	621s	626m	
518s	531w	528s	541m	
541sh	—	—	528sh	
—	—	491vw	—	In-plane and out-of-plane bending, and $T'(Li^{+})$ modes
426w	451m	460m	457w	
—	—	430w	—	
392w	429m	412m	396m	
360sh	403m	364w	368m	
343w	371m	—	340m	
338w	311m	327w	315m	
—	286vw	301s	295vw	
315s	268w	269w	268vw	
274m	260w	—	—	
261w	—	254vw	—	
239sh	235m	241m	248m	Out-of-plane bending, wagging, $T'(In^{3+})$ and L modes
232m	—	231m	—	
227sh	222w	226w	213w	
207m	178m	198w	178w	
194w	—	167m	166vw	
165w	164w	150m	—	
145m	143m	140m	135m	
105w	128w	100w	89m	$T'(MoO_4) \times T'(In^{3+})$
90w	121m	71w	68m	

two In^{3+}, and two $W_2O_8^{4-}$ dimers can be chosen. The results of this analysis are presented in Table 7. In order to facilitate the assignment, the internal vibrations are subdivided into terminal (Mo–O) and bridging (Mo<O>Mo, denoted for simplicity in Table 7 as MoOOMo) modes, where ν denotes stretching and δ bending vibrations. The number of observed modes, 22 in Raman and 24 in IR spectra, is smaller that predicted (see Table 6). Contrary to the high-temperature modification, a number of internal modes show a large Davydov splitting which reflects a strong coupling between MoO_4^{2-} ions within polymeric chains. This feature was reported by us previously for the $NaIn(WO_4)_2$ and $NaSc(WO_4)_2$ crystals (26). By analogy with the sodium compounds, we may assign the strongest Raman line at 966 cm^{-1} to the A_g and the weak 949 cm^{-1} band to the B_g components of the terminal symmetric

TABLE 7
Factor Group Analysis for the Low-Temperature Phase of $LiIn(MoO_4)_2$ ($C2/c$, $Z = 4$)

C_{2h}	n(N)	n(T)	$n(T'(W_2O_8))$	$n(T'(Li))$	$n(T'(In))$	n(L)	n(int)	ν_s(Mo–O)	ν_{as}(Mo–O)	ν_s(MoOOMo)	ν_{as}(MoOOMo)	δ_s(Mo–O)	δ_{as}(Mo–O)	δ_s(MoOOMo)	δ_{as}(MoOOMo)	Activity IR	Activity Raman
A_g	17	0	2	1	1	1	12	1	1	2	2	2	2	1	1	—	xx, yy, zz, xz
B_g	19	0	1	2	2	2	12	1	1	2	2	2	2	1	1	—	xy, yz
A_u	17	1	1	1	1	2	12	1	1	2	2	2	2	1	1	y	—
B_u	19	2	2	2	2	1	12	1	1	2	2	2	2	1	1	x, z	—

stretching mode. The respective IR bands are observed as a doublet at 927–940 cm^{-1}. The terminal asymmetric stretch is observed around 784–797 cm^{-1} and the ν(MoOOMo) modes in the 500–700 cm^{-1} region. Since the normal coordinate calculations, performed for sodium–indium and sodium–scandium double tungstates showed a high degree of coupling among bending and lattice modes (26), the detailed assignment of the observed bands to the respective normal modes is meaningless. We may say only that the 250–500 cm^{-1} bands originate mainly from the in-plane and out-of-plane bending modes coupled to $T'(Li^+)$ modes, whereas the 130–250 cm^{-1} bands may be assigned to coupled out-of-plane bending, $T'(In^{3+})$, and librational modes. The mentioned calculations showed also that the modes below 130 cm^{-1} involved large contribution of translational motions of heavy hexa- and trivalent ions. Our study confirms this conclusion since we observe a significant shift of the two lowest frequency modes toward higher frequency when W atoms are substituted by Mo atoms. This shift is especially well observed in the Raman spectra where the 68 and 89 cm^{-1} modes of $LiIn(WO_4)_2$ (25) shift to 121 and 128 cm^{-1} for $LiIn(MoO_4)_2$ (see Table 6).

Let us now discuss the observed differences in the vibrational properties of $LiIn(MoO_4)_2$ and $LiIn(WO_4)_2$ in detail. The study of a number of molybdates and tungstates showed that Mo–O stretching modes are generally located at lower frequency than W–O stretching modes in isostructural compounds (7). Moreover, the study of $CdW_{1-x}Mo_xO_4$ showed that the substitution of Mo for W in the wolframite structure leads to the shift of the highest frequency IR-active mode toward lower frequency, whereas the position of the highest frequency Raman-active mode is not affected (7). The comparison of the spectra obtained for $LiIn(MoO_4)_2$ and $LiIn(WO_4)_2$ shows that in this case an opposite trend is observed; i.e., the respective modes are observed at much higher frequency in the case of the molybdate than was found for the tungstate (see Table 6). Such an unusual shift of the terminal Mo–O stretching band toward higher frequency results from the fact that the distortion of the MoO_6 octahedra is larger than the distortion of WO_6 octahedra in wolframite-type double compounds. In particular, the length of the shortest M^{VI}–O terminal bond decreases from 1.79(2) Å for $LiFe(WO_4)_2$ (27) to 1.7031(19) Å for $LiIn(MoO_4)_2$ (see Table 3). The observed shift may be predicted on a basis of the valence bond model. This model states that the valence, v_{ij}, of a bond between two atoms i and j is defined so that the sum of all valences from a given atom i with valence V_i obeys (28)

$$\sum_j v_{ij} = V_i. \qquad [1]$$

The most commonly used relation between the bond length d_{ij} and valence is

$$v_{ij} = \exp[(R_{ij} - d_{ij})/B]. \qquad [2]$$

Here B is commonly taken to be a universal constant equal to 0.37 Å and the parameters R_{ij} for bonds between pairs of atoms were tabulated by Brese *et al.* (28). In the case of the Mo–O bonds the expression [2] may be written as

$$v = \exp[(1.907 - d)/0.37]. \qquad [3]$$

Since the Mo atoms in $LiIn(MoO_4)_2$ are on $+6$ oxidation state, for an ideal, regular octahedron the valence per Mo–O bond should be equal to $6/6 = 1$. Using the empirical formula which relates the frequency of a Raman-active Mo–O stretching mode with the bond length (29),

$$d = 0.48239 \ln(32895/\tilde{\nu}), \qquad [4]$$

we may calculate the frequency of the highest terminal Mo–O stretching mode from the measured Mo–O bond length (1.7031(19) Å; see Table 3) to be 963.5 ± 3.8 cm^{-1}. The calculated value is in a very good agreement with Raman study, showing a strong band at 966 cm^{-1}. The respective valence for this bond, calculated with the use of formula [3], is equal to 1.735 ± 0.009. As one can see, in order to fulfil the valence-sum rule [1], the sum of valences for the other five Mo–O bonds in the octahedron must be equal to $6 - 1.735 \pm 0.009 = 4.265 \pm 0.009$. Therefore, the valence per any of the five Mo–O bonds must be much smaller than that found for the shortest bond, and subsequently the respective Mo–O bond lengths must be much longer and the Raman bands should be observed at much lower wavenumbers. This explains the large gap between the 966 cm^{-1} mode and the second strong band, observed at 784 cm^{-1}. As a result of a much stronger distortion of the MoO_6 octahedra in $LiIn(MoO_4)_2$, when compared with the WO_6 octahedra in $LiIn(WO_4)_2$, the observed gap is larger for the molybdate (182 cm^{-1}) than for the tungstate (125 cm^{-1}) (see Table 6).

The observation of a very strong distortion for the MoO_6 octahedra is consistent with the results presented in Ref. 10. In this reference the MoO_6 octahedra were shown to be usually much stronger distorted than WO_6 octahedra (10). This strong distortion was related to the radius of Mo ion which becomes, for $+6$ oxidation state, too small for coordinating of six oxygen atoms (10). The difficulty in the formation of octahedral coordination by Mo atoms may explain the instability of wolframite-type structures for the double and simple molybdates, although such structures are common among tungstates. It is also worth noticing that although the high-temperature polymorph of $LiIn(MoO_4)_2$ is colorless, the low-temperature phase is pale brown. The gradual change in color with pressure was observed previously for $KY(MoO_4)_2$ and $KDy(MoO_4)_2$ and was attributed to backtransfer of charge from oxygen to the molybdenum d orbital (30). This type of effect is known to be observed in strongly stressed crystals, where the stress is sufficient to move electrons from the compressed to stretched cations and to stabilize an unexpected oxidation

state (31). In our case, this explanation is, however, not appropriate since the valence of the Mo atom calculated with the use of formulas [1] and [3], and bond lengths obtained from the X-ray analysis, is equal to 5.99 and agrees with the formal oxidation state + 6. The observed coloration is due, therefore, most likely to the presence of a large number of oxygen vacancies in the obtained crystals, and therefore may reflects the difficulty in coordinating of six oxygen atoms by molybdenum atom. Finally, we would like to point out that although the difference in the ionic radius of Mo^{VI} and $M^{III} + M^{I}$ ions is the key parameter responsible for the stability of wolframite-type structure, some other effects must also play important roles since $LiM^{III}(MoO_4)_2$, where M^{III} = Al, Cr, Ga, Fe, do not form a wolframite-type phase at ambient temperature (32) even though these M^{III} ions are much smaller than In^{III} ones. Moreover, in spite of similarity between ionic radii of In^{III} and Sc^{III}, the lithium–scandium double molybdate seems to be very unstable since our attempt to obtain this compound resulted in formation of mixture containing $Li_3Sc(MoO_4)_3$ and $Sc_2(MoO_4)_3$.

CONCLUSIONS

The results of IR and Raman investigations of the low- and high-temperature phases of $LiIn(MoO_4)_2$ have been presented for the first time. The assignment of observed bands has been proposed. It has been shown that the first-order reconstructive transition leads to the collapse of the structure and as a result the coordination of Mo atoms changes form tetrahedral to octahedral in the high- and low-temperature phase, respectively. The low-temperature structure was shown to be isomorphic to the structure of $LiIn(WO_4)_2$. However, this structure seems to be very unstable due to the smaller ionic radius of the Mo^{VI} atoms in comparison with the W^{VI} atoms. As a result of this instability, the MoO_6 ocahedra are unusually strongly distorted (in comparison with the WO_6 octahedra) and a large number of defects is created, resulting in a pale brown coloration of the crystal.

ACKNOWLEDGMENT

This work was supported by the Polish State Committee for Scientific Research, Grant 3 TO9B 090 15.

REFERENCES

1. T. Ono, N. Ogata, and Y. Miyaro, *J. Catal.* **161,** 78 (1996), and references therein.
2. K. Petermann and G. Gruber, *J. Lumin.* **31 and 32,** 71 (1984).
3. V. Ya. Molchanov, *Proc. SPIE-Int. Soc. Opt. Eng.* **2643,** 189 (1995).
4. A. Sakai, E. Islam, A. Onodera, and B. A. Strukov, *Ferroelectrics* **203,** 87 (1997).
5. J. Simon, J. Banys, J. Hoentsch, G. Volkel, R. Bottcher, A. Hofstaetter, and A. Scharmann, *J. Phys. Cond. Matter* **8,** L359 (1996).
6. A. W. Sleight and L. H. Brixner, *J. Solid State Chem.* **7,** 172 (1973).
7. M. Daturi, G. Busca, m. M. Borel, A. Leclaire, and P. Piaggio, *J. Phys. Chem.* **B101,** 4358 (1997).
8. P. V. Klevtsov, A. V. Demenev, and R. F. Klevtsova, *Sov. Phys. Crystallogr.* **16,** 440 (1971).
9. P. V. Klevtsov and R. F. Klevtsova, *J. Solid State Chem.* **2,** 278 (1970).
10. L. E. Depero and L. Sangaletti, *Phys. Rev.* **B54,** 15678 (1996).
11. P. P. Cord, P. Courtine, and G. Pannetier, *Spectrochim. Acta* **28A,** 1601 (1972).
12. G. W. Smith, and J. A. Ibers, *Acta Crystallogr.* **19,** 269 (1965).
13. P. Courtine, P. P. Cord, G. Pannetier, J. C. Daumas, and R. Montarnal, *Bull. Soc. Chim. Fr.* **12,** 4816 (1968).
14. P. V. Klevtsov, L. P. Kozeeva, and L. Yu. Kharchenko, *Sov. Phys. Crystallogr.* **20,** 732 (1975).
15. N. N. Smyrnagina, N. M. Kozhevnikova, F. P. Alekseev, and M. V. Mokhosoev, *Zh. Neorg. Khimi* **28,** 1582 (1983).
16. Yu. A. Velikodnyi, V. A. Efremov, and V. K. Trunov, *Sov. Phys. Crystallogr.* **25,** 95 (1980).
17. G. M. Sheldrick, SHELX-97 Program for the Refinement of Crystal Structures.
18. L. P. Soloveva and S. V. Borisov, *Sov. Phys. Crystallogr.* **15,** 493 (1970).
19. M. E. Poloznikova, O. I. Kondratov, N. G. Chaban, V. V. Safonov, and V. V. Fomichev, *Zh. Neorg. Khim.* **34,** 655 (1989).
20. M. Maczka, J. Hanuza, E. T. G. Lutz, and J. H. van der Maas, *J. Solid State Chem.* **142,** 751 (1999).
21. M. Maczka, *Eur. J. Solid State Inorg. Chem.* **33,** 783 (1996).
22. Yu. A. Velikodnyi, V. K. Trunov, and N. I. Markelova, *Zh. Neorg. Khim.* **15,** 3046 (1970).
23. P. V. Klevtsov, and R. F. Klevtsova, *Zh. Strukt. Khim.* **18,** 419 (1977).
24. V. V. Fomichev, and O. I. Kondratov, *Spectrochim. Acta* **50A,** 1113 (1994).
25. M. Maczka, *J. Solid State Chem.* **129,** 287 (1997).
26. J. Hanuza, L. Macalik, M. Maczka, E. T. G. Lutz, and J. H. van der Maas, *J. Mol. Struct.* **511–512,** 85 (1999).
27. P. V. Klevtsov, and R. F. Klevtsova, *Sov. Phys. Crystallogr.* **15,** 245 (1970).
28. N. E. Brese and M. O'Keeffe, *Acta Crystallogr. B* **47,** 192 (1991).
29. F. D. Hardcastle and I. E. Wachs, *J. Phys. Chem.* **95,** 10763 (1991).
30. A. Jayaraman, S. K. Sharma, S. Y. Wang, S. R. Shieh, L. C. Ming, and S.-W. Cheong, *J. Raman Spectrosc.* **27,** 485 (1996).
31. I. D. Brown, *Acta Crystallogr. B* **48,** 553 (1992).
32. P. V. Klevtsov, *Sov. Phys. Crystallogr.* **15,** 682 (1970).